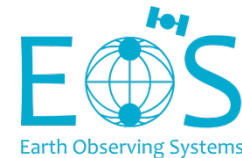


Dragon Sea Ice Remote Sensing – Preparations of Future Activities

Wolfgang Dierking
Alfred Wegener Institute
&
Arctic University of Norway

In collaboration with
Xi Zhang, First Institute of Oceanography , Qingdao



Sea Ice Deformation

Inhomogeneous drift of sea ice

Sea ice deformation/stress

Causes:

Opening / closing of leads

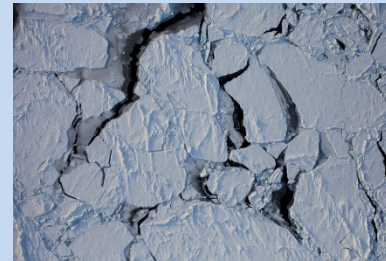


Formation of shear- or pressure- ridges



Results in:

Change of sea ice concentration



Change of sea ice thickness



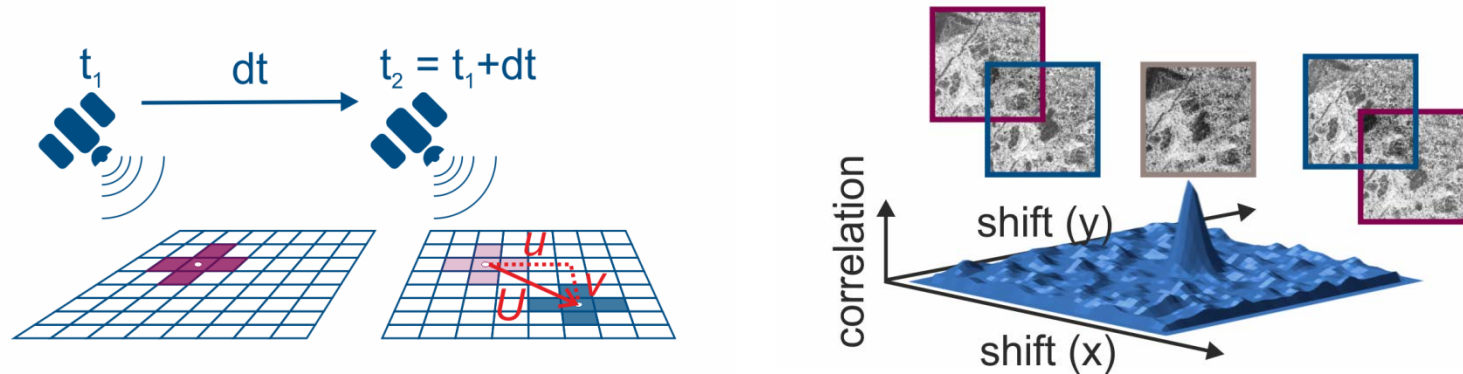
Affects:

Navigation of the marine traffic in polar regions

Interaction between atmosphere, ice, and ocean

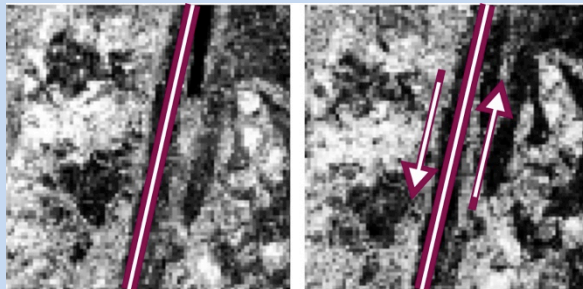
Detection of Drift- & Deformation

Sea ice pattern matching algorithms → retrieval of the sea ice drift field

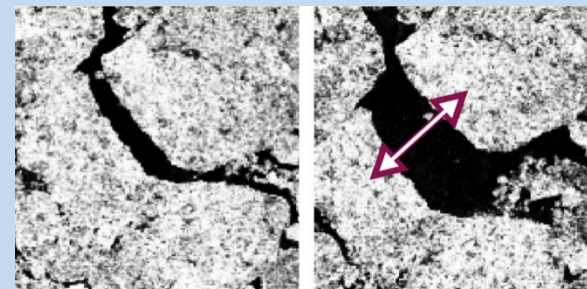


Sea ice deformation causes temporal variations of recognizable patterns

Example: Shear



Example: Divergence



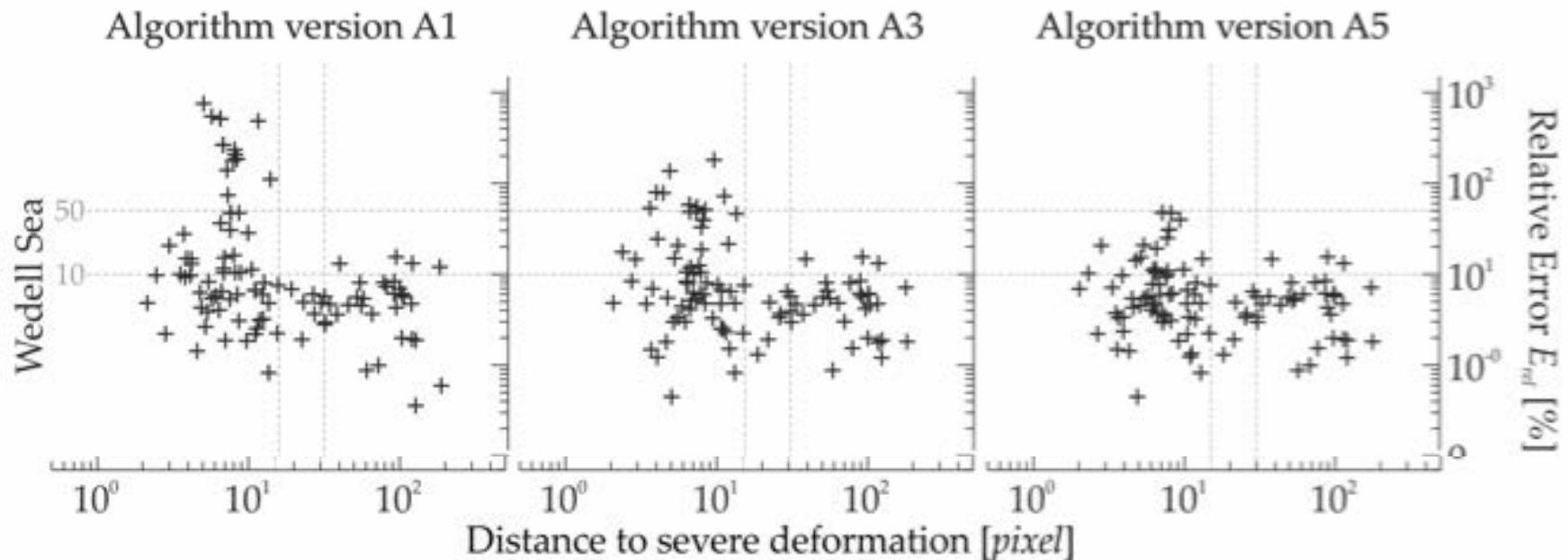
Drift-detection algorithm have to take sea ice deformation into account

Viewgraph prepared by Jakob Griebel, AWI

Detection of Drift- & Deformation



Improvement of algorithm through explicitly considering deformation patterns



A1 – pattern matching, A3 = A1+median filter and reliability assessment,
A5 = A1+reliability assessment + segmentation of windows around deformation zones

Griebel, J., Dierking, W., A method to improve high-resolution sea ice drift retrievals in the presence of deformation zones, Remote Sensing 2017 (under review, minor revisions)

Characteristics of Ice Ridges (1)

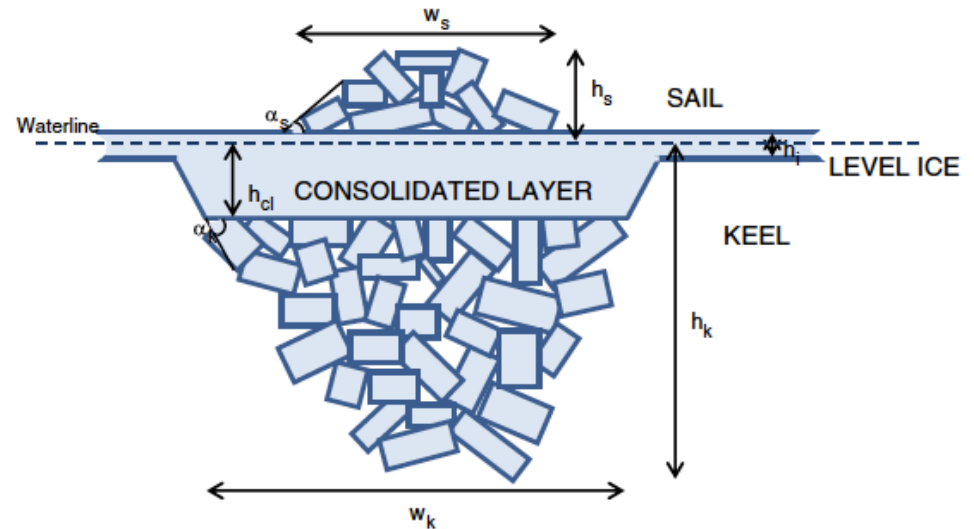
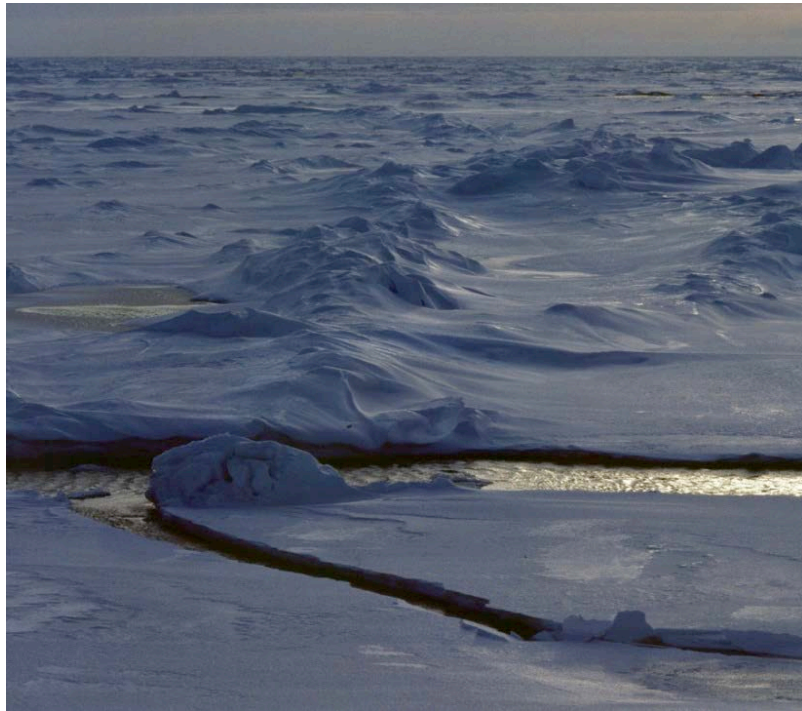
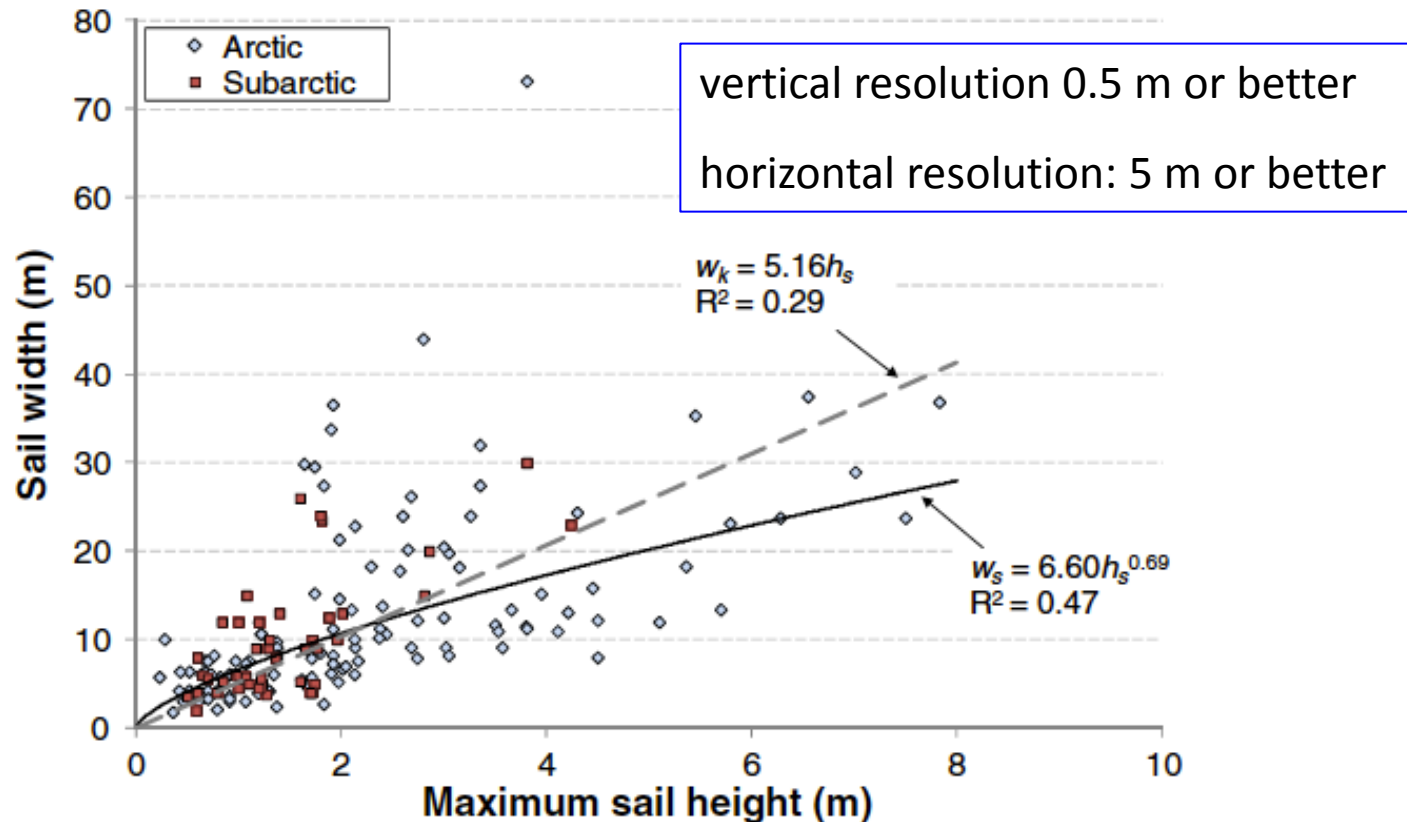


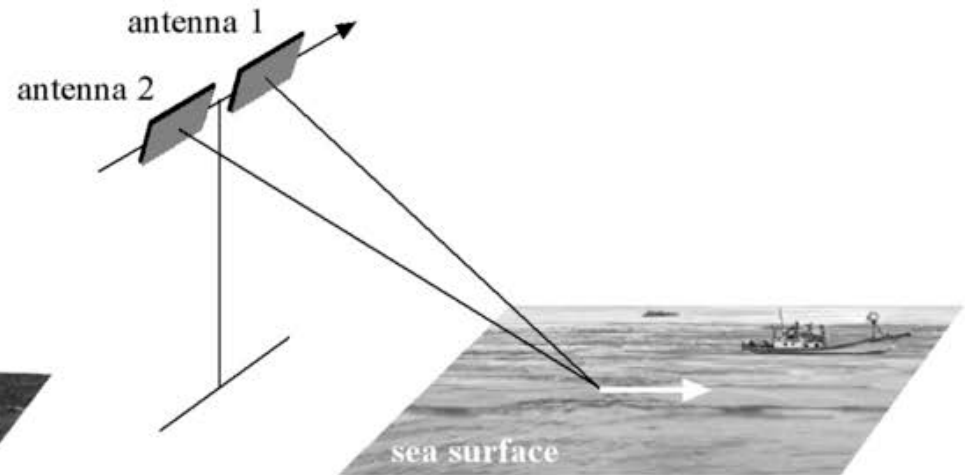
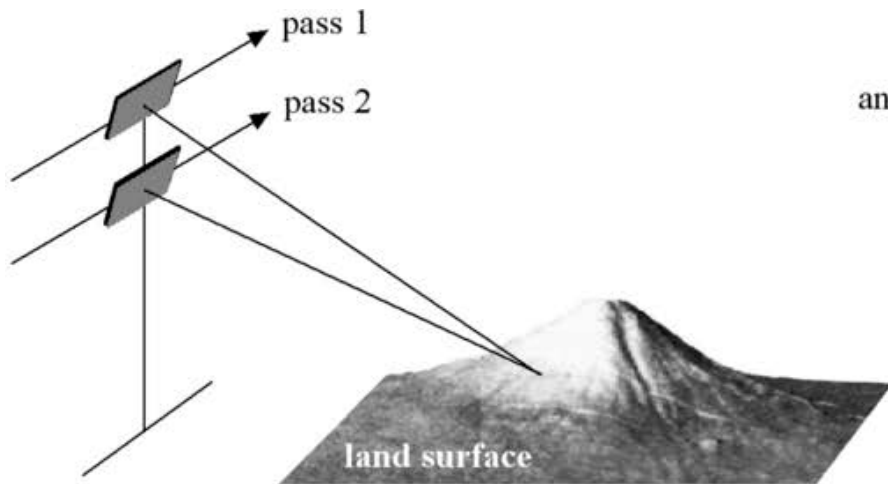
Fig. 1. Typical model of a first-year ice ridge.

Characteristics of Ice Ridges (2)



Strub-Klein & Sudom, Cold Regions Science and Technology 82, 2012

Using Interferometric SAR?



Across-track and along-track interferometry

- sensitive to topography
- not sensitive to motion
- sensitive to movements
- not sensitive to topography

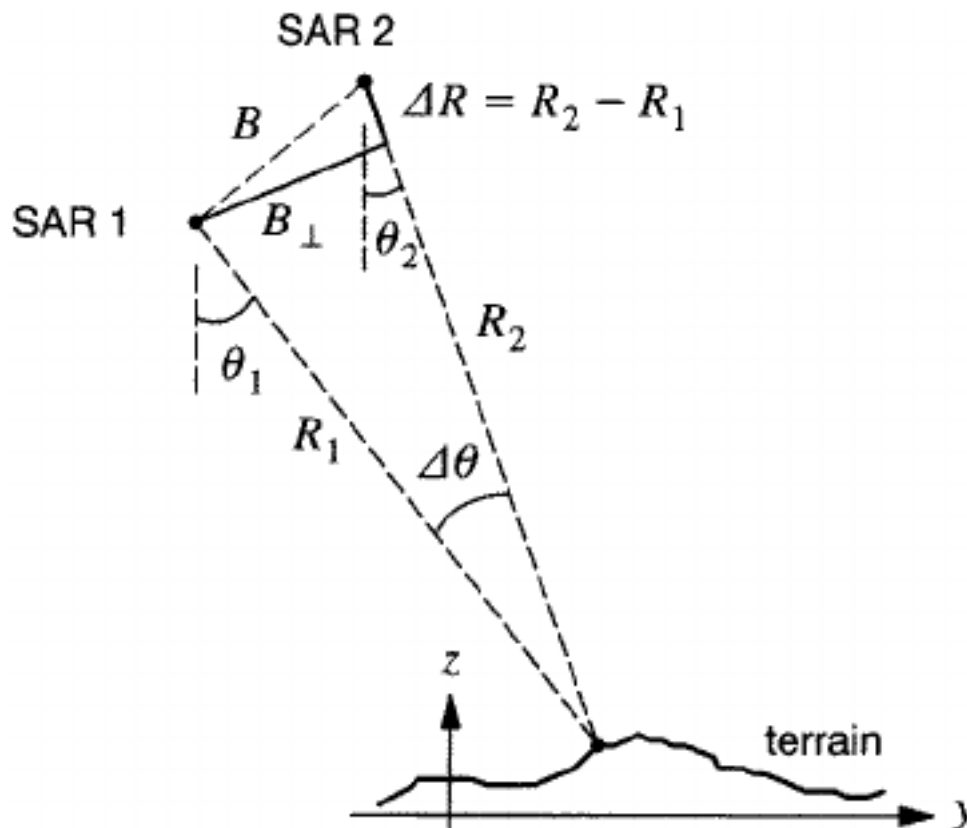
InSAR: numbers for different mission scenarios?

Band	L		C		X		K _u		K _a	
λ [m]	0.24		0.055		0.031		0.022		0.0084	
H [km]	745 km		700		500		780		740	
θ [deg]	25	40	25	40	25	40	25	40	25	40
Δy [m]	4.2	2.7	4.6	5.0	2.8	1.9	3.5	2.3	8.9	5.8
B_{cn} [km]	52	112	10.2	13.1	6.7	13.9	6.0	12.7	0.85	1.8
B_n [km]	19.8	43.1	3.9	5.0	2.6	5.3	2.3	4.9	0.32	0.69
h_a [m]	4.2	3.5	4.6	6.4	2.8	2.4	3.5	3.0	8.9	7.5
σ_h [m]	0.60	0.50	0.66	0.92	0.40	0.35	0.50	0.42	1.3	1.1

Table 1: Ambiguity heights h_a and relative height errors σ_h (rounded values) for optimal baselines B_n , determined for different satellite configurations (λ – radar wavelength, H – orbit height, θ – radar incidence angle, Δy – ground range resolution). It is assumed that $p=1$, $N_L = 1$, and $\gamma_N \approx 1$ in equations 2, 4, and 8.

Dierking et al., The Cryosphere Discussions, 2017

Interferometric Baseline And Height Sensitivity

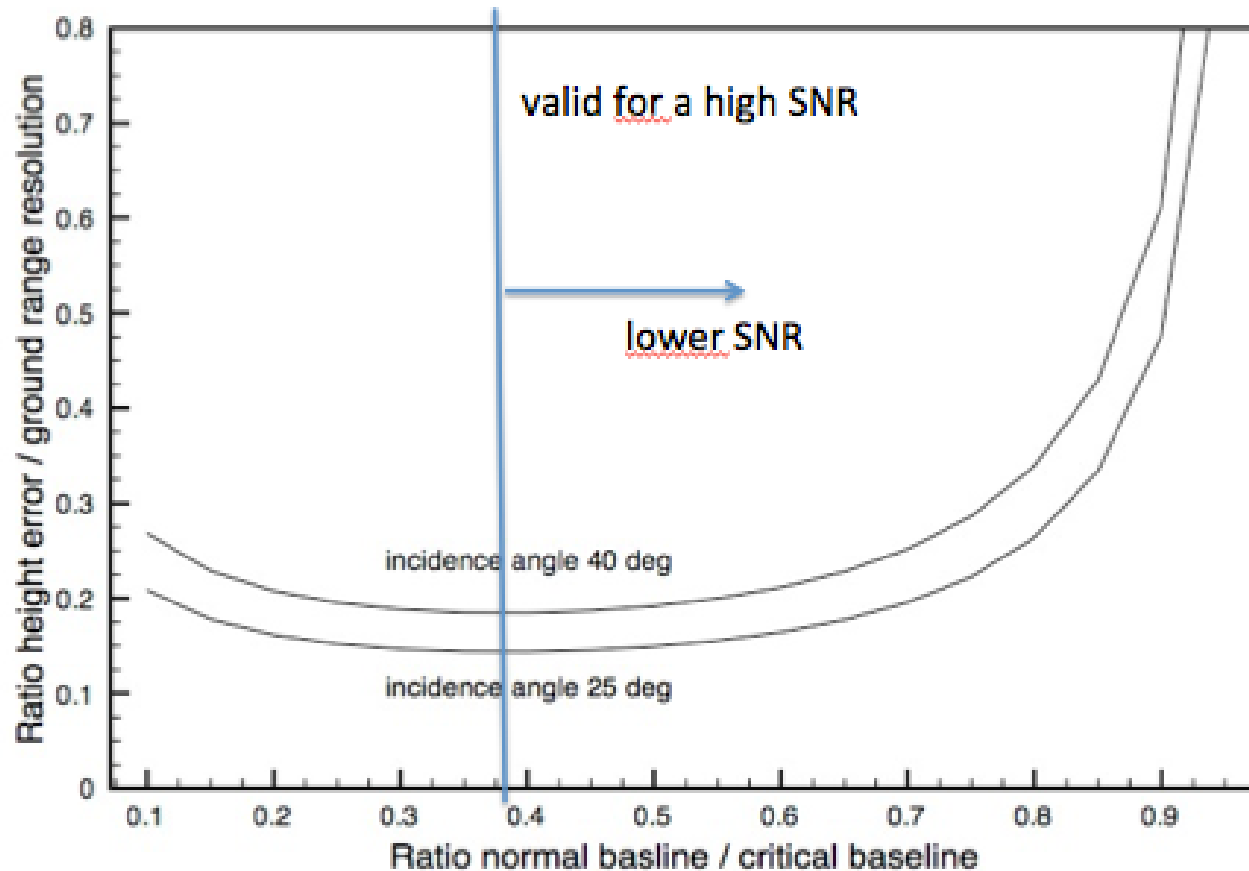


Favourable conditions for retrieval of surface elevation:

- long baseline B_n
- short radar wavelength
- low orbit
- steep incidence angle

BUT: critical baseline
=> loss of coherence!

Optimal Baseline (1)



Dierking et al., The Cryosphere Discussions, 2017

Optimal Baseline (2)

Band	L		C		X		K_a		K_a	
λ [m]	0.24		0.055		0.031		0.022		0.0084	
H [km]	745 km		700		500		780		740	
θ [deg]	25	40	25	40	25	40	25	40	25	40
Δy [m]	4.2	2.7	4.6	5.0	2.8	1.9	3.5	2.3	8.9	5.8
B_{cn} [km]	52	112	10.2	13.1	6.7	13.9	6.0	12.7	0.85	1.8
B_n [km]	19.8	43.1	3.9	5.0	2.6	5.3	2.3	4.9	0.32	0.69
h_a [m]	4.2	3.5	4.6	6.4	2.8	2.4	3.5	3.0	8.9	7.5
σ_h [m]	0.60	0.50	0.66	0.92	0.40	0.35	0.50	0.42	1.3	1.1

Optimal Baseline (2)

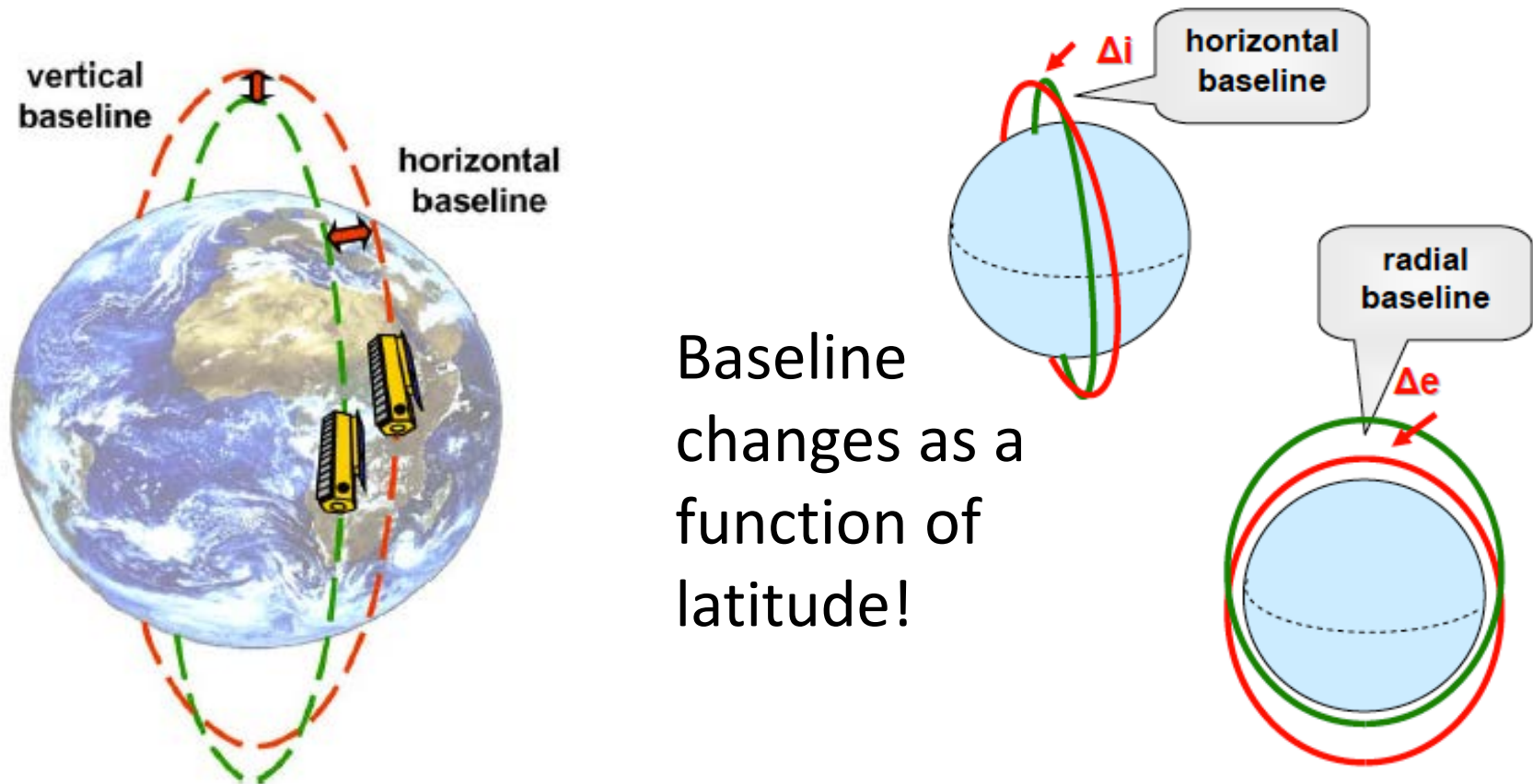
Single satellite platform possible?

Perhaps Ka-band(?) Otherwise: no way!

Satellite tandem required!

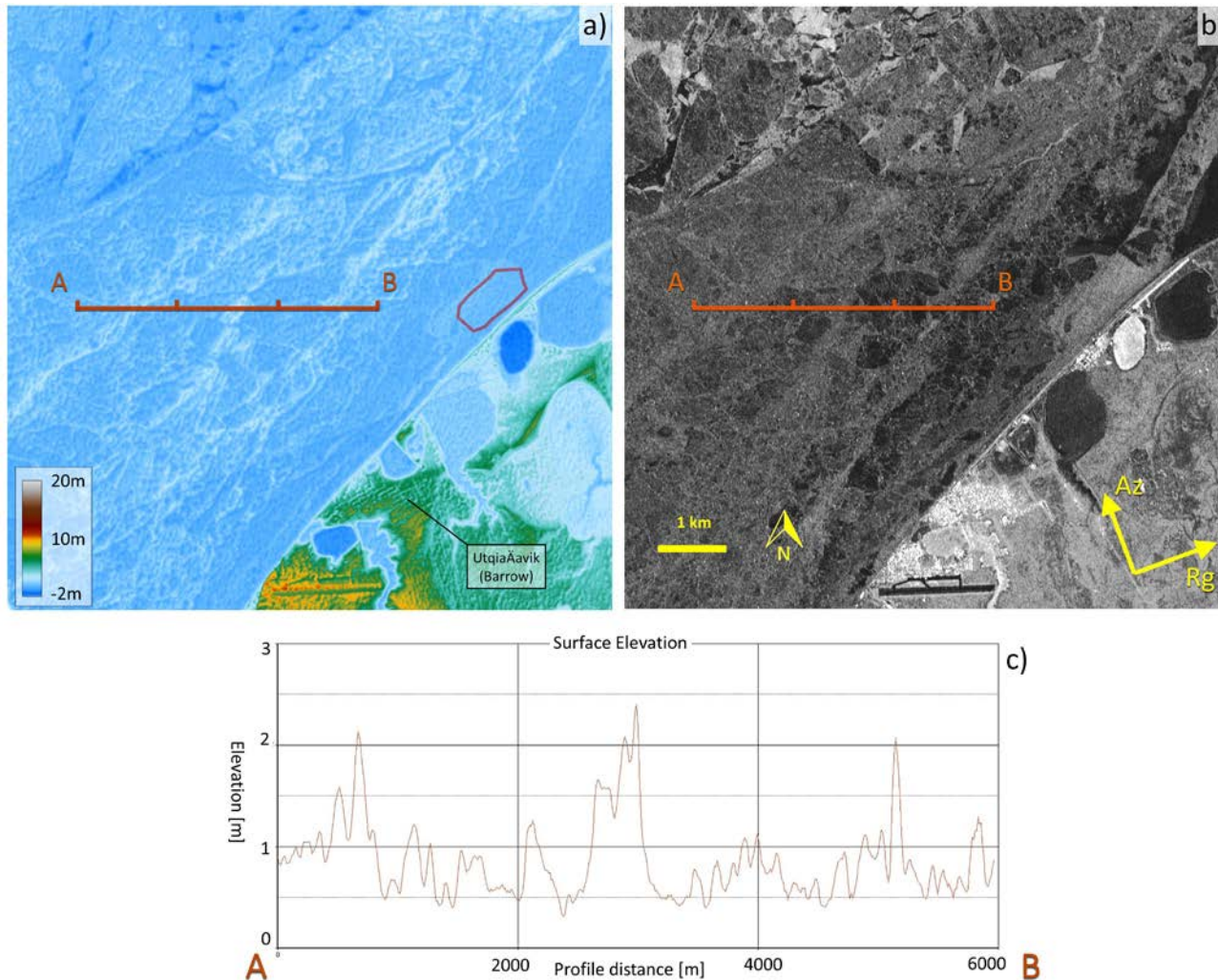
Band										K_a
λ [m]										0.0084
H [km]										740
θ [deg]										5 40
Δy [m]										9 5.8
B_{cn} [km]	52	112	10.2	13.1	6.7	13.9	6.0	12.7	0.85	1.8
B_n [km]	19.8	43.1	3.9	5.0	2.6	5.3	2.3	4.9	0.32	0.69
h_a [m]	4.2	3.5	4.6	6.4	2.8	2.4	3.5	3.0	8.9	7.5
σ_h [m]	0.60	0.50	0.66	0.92	0.40	0.35	0.50	0.42	1.3	1.1

Realization of Large Normal Baselines in Space (1)



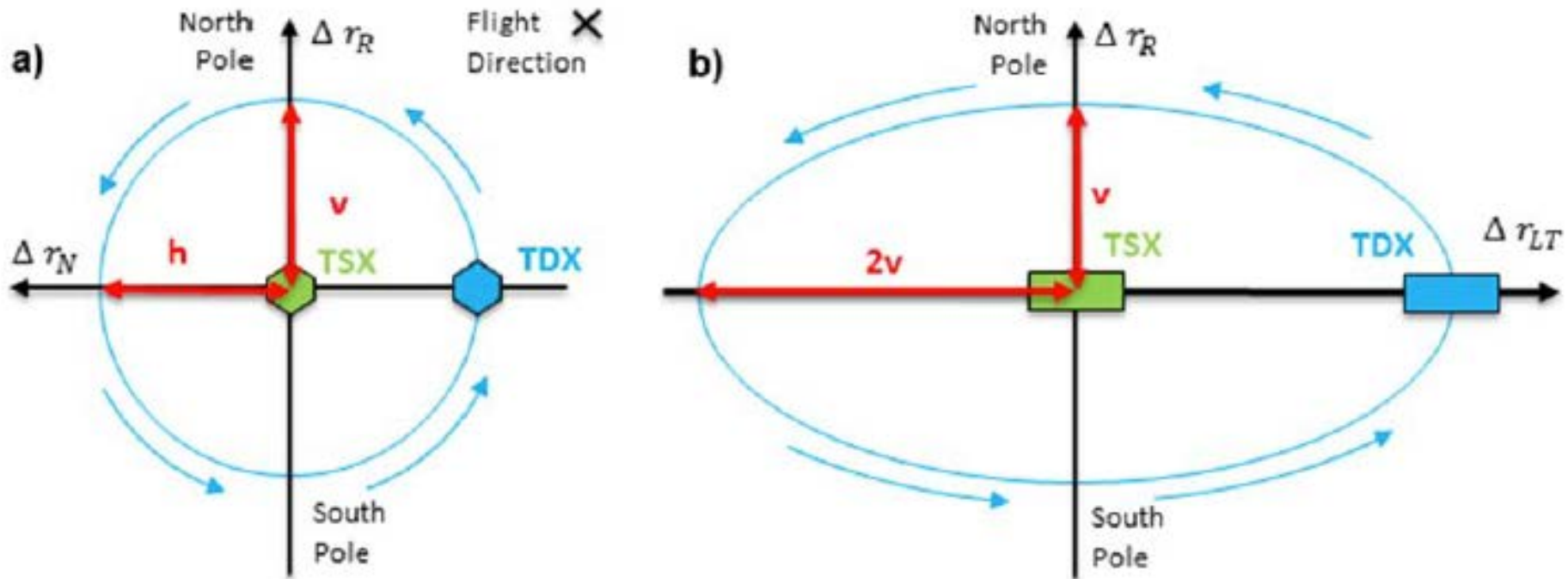
Krieger et al., Trans. Geoscience and Remote Sensing, Vo. 45, No. 11, 2007
Krieger et al., presentation Fringe 2009

Tandem-X Science Phase: Landfast Ice Surface Topography



Dierking et al.,
The Cryosphere,
2017

Realization of Larger Normal Baselines in Space (2)



Tandem-X bistatic mode:
 along-track baseline variation between $\pm 2 \times$ vertical baseline
Example: VB 300m, ATB 0 at poles, $\pm 600\text{m}$ at equator

Maurer et al., SpaceObs Conference, Korea 2016

Influence of Along-Track Baseline

$$\Delta\phi = \Delta\phi_{topo}(B_{ac}) + \Delta\phi_{mov}(B_{al}) + \Delta\phi_{noise} + 2\pi n$$

Critical ATB causing phase shifts => 0.5m height change

Band	L		C		X		K _u		K _a	
v [km/s]	7.0		6.7		7.0		7.0		6.7	
u_{LOS} [m/s]	0.05	0.6	0.05	0.6	0.05	0.6	0.05	0.6	0.05	0.6
B_{al} [m]	3360	280	737	61	434	36	308	26	112	9.4
B_{al} [s]	0.480	0.04	0.11	0.009	0.062	0.005	0.044	0.004	0.017	0.0014

Movement or topography?

Dierking et al., The Cryosphere Discussions, 2017